Journal Pre-proofs

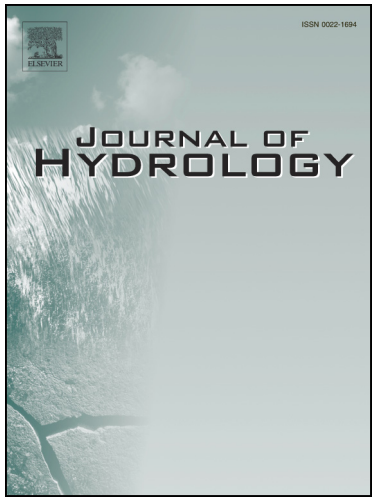

Research papers

Paleoflood Hydrology on the lower Green River, upper Colorado River Basin, USA: An Example of a Naturalist Approach to Flood-Risk Analysis

Tao Liu, Noam Greenbaum, Victor R. Baker, Lin Ji, Jill Onken, John Weisheit, Naomi Porat, Tammy Rittenour

PII: S0022-1694(19)31027-3
DOI: https://doi.org/10.1016/j.jhydrol.2019.124292
Reference: HYDROL 124337

To appear in: *Journal of Hydrology*

Received Date: 16 May 2019
Revised Date: 19 October 2019
Accepted Date: 26 October 2019

Please cite this article as: Liu, T., Greenbaum, N., Baker, V.R., Ji, L., Onken, J., Weisheit, J., Porat, N., Rittenour, T., Paleoflood Hydrology on the lower Green River, upper Colorado River Basin, USA: An Example of a Naturalist Approach to Flood-Risk Analysis, *Journal of Hydrology* (2019), doi: https://doi.org/10.1016/j.jhydrol.2019.124292

Paleoflood Hydrology on the lower Green River, upper Colorado River Basin, USA: An Example of a Naturalist Approach to Flood-Risk Analysis

Tao Liu[1*], Noam Greenbaum[2], Victor R. Baker[1*], Lin Ji[1], Jill Onken[3], John Weisheit[4], Naomi Porat[5], Tammy Rittenour[6]

[1] Department of Hydrology and Atmospheric Sciences, University of Arizona, Tucson, Arizona, USA, 85721-0011.

[2] Department of Geography and Environmental Studies, University of Haifa, Haifa, Israel.

[3] Department of Geosciences, University of Arizona, Tucson, Arizona, USA.

[4] Living Rivers, Moab, Utah.

[5] Laboratory of Luminescence Dating, Geological Survey of Israel, Jerusalem, Israel.

[6] Department of Geology, Utah State University, Logan, Utah, USA.

Corresponding author: Tao Liu (liutao@email.arizona.edu) and Victor R. Baker (baker@email.arizona.edu)

Abstract

Through a comprehensive paleoflood hydrological investigation we document natural evidence for at least 27 high-magnitude paleofloods at six sites on the Lower Green River, Utah. Hydraulic analysis, using the Sedimentation and River Hydraulic-2D model (SRH-2D), shows that the responsible peak paleoflood discharges ranged between 500 and 7500 m^3/s. At least 14 of these paleoflood discharge peaks exceed a level twice that of the maximum systematic record of gauged flows: 1929 m^3/s. Geochronological analyses, employing optically stimulated luminescence (OSL) and radiocarbon dating techniques, demonstrate that these 14 largest paleoflood peaks occurred during the past 700 years. Integration of the paleoflood data into flood frequency analyses (FFA) reveals considerably higher values for the upper tails of the flood distribution than does a FFA based solely on the systematic gauged record, indicating that extreme floods are larger and more frequent than implied by the relatively short gauged record. Through examination of three approaches to extreme flood estimation – conventional FFA, probable maximum flood estimation (PMF), and paleoflood hydrology (PFH) – we show the significance of the natural evidence for advancing scientific understanding of extreme floods that naturally occur in the Colorado River system. We argue that this kind of scientific understanding is absolutely essential for achieving a credible evaluation of extreme flood risk in a watershed of immense importance to economic prosperity of the southwestern U.S.

Keywords:

Paleoflood hydrology; Flood-Risk Analysis; Naturalist Approach; Green River; upper Colorado River Basin

1 Introduction

1.1 Background/Problem:

Floods result in many of the most frequent and costly water-related natural disasters worldwide. Their global impacts include losses of life and billions of dollars in financial damages. Over the past century, national stream gauging networks were established in many countries to provide systematic and quantitative data on streamflow, including flooding. To make effective use of the resulting accumulation of hydrological and meteorological observations two primary methodologies were developed, mainly in the engineering community: flood-frequency analysis (FFA) and probable maximum flood (PMF) estimation, (National Environment Research Council, 1999; SL44-2006).

Conventional FFA combines systematical records with statistical/mathematical theories to provide actionable information for flood risk assessment. This is conducted by fitting functions to peak annual discharges obtained from gauged records for a drainage basin. Extrapolations are made from what is usually a very short instrumental flood record of relatively small flood peaks in order to estimate flood extremes that may have very long return periods. In other words, extreme flood estimates are based on the statistical properties of the relatively frequent, small-scale flooding that is most commonly represented in gauge records. It therefore is a matter of assumption that this record can be reliably extrapolated upscale to predict the magnitudes of unknown rare, extremes. A key FFA assumption is that the flood peaks are independently, identically distributed (iid), because this "iid" criterion is a necessity for achieving valid statistical inferences (Kesiel, 1969). However, in areas of high flood variability, such as the southwestern U.S., peak flood series are commonly mixed distributions, such that the most extreme flood peaks are generated by very different meteorological phenomena than are the

less extreme peaks (Hirschboeck, 1998). Though these and other shortcomings have been obvious for decades (Klemes, 1996), conventional FFA continues to be utilized as a matter of standard practice, often in ignorance that opportunities may be available to overcome shortcomings in regard to making credible extrapolations to flood extremes.

PMF procedures, like FFA, can be lacking in credibility. These procedures employ hydrological models that may embody highly problematic presumptions, particularly in regard to conditions representing the most extreme flood-generating parameters. By definition, PMF modeling predicts the most extreme flood peak that could conceivably occur at a particular location, i.e., a prediction of something at the absolute limit of what theoretically is supposed to occur. Were an exceedance of such flooding actually to occur, of course, the model would thereby, be falsified by an act of nature.

As a matter of logical inference, PMF procedures are largely deductive; they can indeed yield true conclusions, but only if the assumptions made are indeed true to reality. In contrast, FFA procedures are largely an inductive, in that various statistical methods are employed to generalize from data and address associated uncertainties. While these approaches have long applied engineering traditions in both empirical and theoretical hydrology, they also have limitations in regard to hydrology viewed as a complete scientific discipline (Baker, 2017). This paper employs a third mode of reasoning, abduction, which works in concert with both deduction and induction to generate enhanced understanding of the nature of extreme floods (Baker, 1996, 1998).

1.2 Paleoflood hydrology

Paleoflood hydrology (PFH) relies on the identification of physical evidence of past flood phenomena, including flood slackwater deposits and related paleostage indicators (SWD-PSIs)

that serve as high-water marks (HWMs) (Baker, 1987). SWD-PSIs are used to determine the associated flood magnitudes through the application of hydraulic principles (Baker, 2008; Benito and O'Connor, 2013). PFH results can provide both (1) a sound foundation for flood-frequency analysis (Costa, 1978; Baker et al., 1979, 2002; Stedinger and Baker, 1987) and (2) hydrological model improvements (England et al., 2014). PFH also provides real-world flood data with which to inform the search for flood-climate linkages in a broad context, as global and regional atmospheric circulation patterns and processes drive changing flood-generating meteorological elements over long time scales (Ely et al., 1993; Knox, 2000; Benito et al., 2003, 2015; Macklin, 2006; Huang et al., 2007; Harden et al., 2010; Merz et al., 2014; Toonen et al., 2017; Wilhelm et al., 2018, 2019).

PFH was embraced for both scientific and engineering applications worldwide after early programs of paleoflood investigation were initiated in central Texas during the 1970s (Baker, 1975; Patton and Baker, 1977) and subsequent paleoflood studies were accomplished in the broader Southwestern U.S. (Patton and Dibble, 1982; Kochel et al., 1982; Ely and Baker, 1985; Webb et al., 1988; Jarrett, 1990; O'Connor et al., 1994; Ostenaa et al., 1996), and then in other parts of the North America (Knox, 1985, 1993, 2000; Springer and Kite, 1997; Brown et al., 2000; Saint-Laurent et al., 2001; O'Connor et al., 2003). Applications outside of the U.S. include Australia (Pickup et al., 1988), Spain (Benito et al., 2003), France (Sheffer et al. 2008), China (Huang et al., 2010; Liu et al., 2014), Japan (Jones et al., 2001), India (Kale et al., 1997), Thailand (Kidson et al., 2005), and Israel (Wohl et al., 1994; Greenbaum et al., 2000; 2006).

The Colorado River is the most important river in the southwestern U.S., providing water for municipal drinking water, agriculture irrigation systems, and hydropower needs for more than 35 million people in seven states. Extreme flooding along this river would also cause massive

disasters along floodplains and bring about severe damage to infrastructure and high economic costs, including the potential loss of major dams that are critical to the economy of the entire region. A large number of paleoflood investigations have been conducted in the lower Colorado River and its tributaries (e.g., Ely and Baker, 1985; Partridge and Baker, 1987; Fuller, 1987; Enzel et al., 1994; Webb et al., 1988; O'Connor et al., 1994). These studies and subsequent syntheses (Enzel et al., 1993; Harden et al., 2010) provide for robust knowledge of real-world floods that have actually occurred over the last several thousand years. In contrast, there have been relatively few paleoflood studies conducted in the upper Colorado River Basin, where more than 95% of the Colorado River's discharge originates (Blinn and Poff, 2005). An important exception is the study by Greenbaum et al., (2014) which found natural evidence for 44 extreme floods occurring during the last 2000 years on the upper Colorado River, near Moab, Utah. Two of these paleofloods exceeded the PMF of 8500 m3/s, and the whole assemblage of largest paleoflood peaks was found to be more frequent than could be estimated on the basis of the systematic gauge data alone. Given this example of combining long-term paleoflood records with high spatial-temporal resolution systematic observations, and their linkages to climate change, we hope further to advance understanding extreme flood generation mechanism and improve upon estimates for the occurrences and magnitudes of future extreme flooding in the upper Colorado River Basin.

In this study, we present the results of investigations along the Stillwater Canyon section of the lower Green River. We document the paleoflood events of the last 700 years, using SWD-PSIs and 2D hydraulic modeling to estimate the associated peak discharges. We then apply these new paleoflood data in FFA using different methodologies. The results are then discussed in

terms of their great potential for gaining understanding of nature of extreme flood events and their linkages with climatic changes in the upper Colorado River Basin.

2 Study area

The Green River is a chief tributary of the upper Colorado River. It is 1,170 km long and has a drainage area of 124,600 km^2 that includes parts of Wyoming, Utah, and Colorado (Figure 1). It contributes nearly half of the total annual flow to the Colorado River at the confluence. Heading in the Wind River Range of Wyoming, the Green River receives tributary flows from western Colorado, then flows south through the Uinta Mountains and the Uinta Basin of Utah, finally traversing a long series of canyons before joining the main stem of the Colorado River in south-central Utah. In its lower reaches from the town of Green River UT to the junction with the Colorado River, the Green River meanders through steep, stable sandstone bedrock canyons (Cashion, 1967), Labyrinth and Stillwater, where gradients approach 0.1 m/km. The Green River joins the Colorado River roughly 63 km downstream of Moab, UT.

Figure 1. Green River Basin including the large tributaries, USGS gauging station, and the study reach.

Precipitation in the upper Green River Basin can exceed 1000 mm water equivalent per year, with most of this generally occurring in the form of winter snow. In contrast, the lower Green River Basin has a semiarid climate characterized by cold winters and hot, dry summers. NOAA COOP station (No. 421163) in Canyonlands National Park (1965-2018, Western Regional Climate Center, 2013) records the in-situ climate variables. The records indicate annual mean temperature is 5.78 ℃ with the maximum monthly mean temperature in July, varying between 18.8 and 32.6 ℃, and the minimum monthly mean temperature in January, varying

between -6.3 and 2.7 ℃. Annual mean precipitation is 229 mm, ranging between 117 and 338 mm. This precipitation is attributed to 1) summer and fall convective storms coming from the Gulf of Mexico or the Gulf of California, 2) large-scale cyclonic storms resulting from Pacific air masses in summer and fall, and 3) North Pacific frontal storms in winter (Blinn and Poff, 2005).

The USGS gauging station on the Green River at Green River, Utah (No. 09315000) is situated ca. 200 km upstream from the confluence of the Green and Colorado Rivers (Figure 1). The drainage area of the Green River at this location is 116,160 km^2, accounting for 93% of the basin. The gauge has recorded the daily discharge rate since 1894 and is continuous except for the period 1900-1904. At this station, the average annual discharge is 170.0 m^3/s with a maximum of 347.8 m^3/s and minimum of 51.1 m^3/s. The annual maximum gauged flood peaks range from a low of 183 m^3/s in 1934, to a high of 1929 m^3/s in 1917 with an average of 790 m^3/s (Figure 2). Besides the gauged record, there is no humanly recorded historical flood record that we could find for the Green River.

Figure 2. Annual maximum peak discharges on the Green River at the USGS gauging station Green River, Utah, 1894-2016.

This study involves six paleoflood study sites along Stillwater Canyon of the Lower Green River. As the name suggests, this is a canyon that is free of rapids (swift turbulent flow) where the river loops in sinuous curves bedrock meanders. The study sites are distributed unevenly along a 35-km long reach from the mouth of Dead Horse Canyon to the confluence with the Colorado River (Figure 3). The river channel averages about 250–350 m in width and flows within a ~120 m deep canyon with near vertical fully bedrock walls.

Figure 3. A map showing six study sites (DHC, RF, LS, HD, HB, and PC) on the Lower Green River (left), the stratigraphic illustrations showing the paleoflood slackwater deposit layers

(black lines) and the river channel and valley dimensions of each stratigraphic section (middle), and the cross-sections at each site (right), showing the range of extreme flood water surface elevation.

3 Methodologies

3.1 Paleoflood Record Analysis

There are many techniques available for making inferences concerning the hydrological parameters for past flood events, employing principles of geomorphology and related aspects of Quaternary stratigraphy and sedimentology (Baker, 2008; England, 2010). The most accurate method involves slackwater deposits and paleostage indicators (SWD-PSI) in stable-boundary fluvial reaches (Baker, 1987). Slackwater deposits are fine grained sediments, mainly sand, conveyed in suspension during highly energetic flood flows and deposited in areas of flow separation that result in long-term preservation after the flood recession (Baker, 2008). During our detailed field paleo-hydrological investigations layered sequences of slackwater deposits were found at the six study sites along Stillwater Canyon of the lower Green River (Figure 3). The paleoflood SWDs include between 7-11 flood deposits at most of the sections with one section containing only two SWDs while another contained 30 SWDs (Figure 4). Sites are located up to 13.5 m above water level (a.w.l.). We exposed stratigraphic sections at each site, made detailed descriptions of the flood SWDs, and sampled for OSL and radiocarbon dating. The sedimentary units associated with paleoflood events were identified using the well-established sedimentological criteria (Baker, 1987; Kochel and Baker, 1988; House et al., 2002; Benito and O'Connor, 2013).

Figure 4. Stratigraphic section at Dead Horse Canyon (DHC) site and Rock Fall (RF) site.

3.2 Paleoflood Age Determination

We employed two geochronology techniques to develop a robust paleoflood chronology: Accelerator Mass Spectrometry (AMS) radiocarbon (^{14}C) dating of charcoal and plant material and optically stimulated luminescence (OSL) dating of quartz sand. Radiocarbon dating is the most widely used geochronology method in fluvial studies, and the analytical techniques have been highly refined over the past several decades. Three ^{14}C samples were collected at two of six sites to estimate ages of the SWDs. The samples were prepared and analyzed at the Arizona AMS Lab at The University of Arizona, with calibration to calendar years (OXCAL 4.3), using the IntCal13 calibration curve (Reimer et al. 2013) and reported as two-sigma calibrated age ranges (Table 2). Because of insufficient amounts of the organic matter, most of this study employed OSL dating. Twelve OSL samples were submitted to the Dating Laboratory of the Israel Geological Survey in Jerusalem, and three were analyzed at the Luminescence Lab at the Utah State University. We employed the latest single-aliquot regenerative-dose (SAR) procedures for OSL dating of quartz sand (Murray and Wintle, 2000, 2003; Wintle and Murray, 2006). Dose-rate calculations were determined by chemical analysis of the U, Th, K and Rb content using ICP-MS and ICP-AES techniques and conversion factors from Guérin et al. (2011). The contribution of cosmic radiation to the dose rate was calculated using sample depth, elevation, and latitude/longitude following Prescott and Hutton (1994). Dose rates are calculated based on water content, sediment chemistry, and cosmic contribution (Aitken and Xie, 1990; Aitken, 1998).

3.3 Paleoflood hydraulic analysis

Paleoflood discharge estimation can be accomplished by methods ranging from simple hydraulic formulae applied at a single cross-section to a variety of one-, two- or even three-

dimensional hydraulic modeling codes applied to high-resolution channel geometry data. For this study, we used the two-dimensional hydraulic model SHR-2D (Sedimentation and River Hydraulics-2D, Lai, 2009) to estimate peak discharges for the paleofloods. Roughness values were identified and delineated within zones for the modeled study reach. The Manning's n values chosen for the hydraulic model are 0.028 for the channel and 0.045 for the banks, based on observations made in the field and comparison to values previously published for a similar reach of the upper Colorado River (Greenbaum et al., 2014). A sensitivity analysis was performed to examine changes in hydraulic calculations response to the uncertainty of roughness coefficient. Mesh cells chosen for the model in the river channel had an approximate size of 2-6 meters, but, where the canyon walls were more widely spaced, we increased the dimensions to between 6 and 8 meters. For areas of interest, especially those near the SWD sites, we employed finer mesh cells to provide more detail. The 2D model results also displayed the water depth and velocity distribution in the study reach, information of importance to understanding the depositional environment of SWDs.

The downstream boundary condition set in the model for each flow estimate was normal depth. The location of the downstream boundary was established far enough downstream so that any uncertainty in this value would not affect model results in areas of interest. The model run was initiated from a dry condition and continued with a two second time step. The simulation time for each modeled flow varied from 10-16 hours, in which time the incoming and outgoing flows and water surface elevation at monitoring points stabilized. LiDAR data were used to develop the geometry of the channel for the hydraulic model, and this provided a high-resolution Digital Elevation Model (DEM) with a 0.5-meter grid spacing and ≤19.6 cm vertical accuracy. The LiDAR scanning happened during the low water season with discharges ranging 26-50 m^3/s.

Depth-recording sonar was used at multiple sections, confirming that water depths were generally less than a meter or so during the low water season.

We input successive discharges for the upstream boundary and obtained discharge-stage (Q-S) relationships for each site. The paleoflood discharges were acquired from the resulting rating curves, which were fitted based on the relevant Q-S relationships. Because the elevation of a SWD is somewhat lower than the actual water surface during the flooding, the reconstructed discharge is treated as the minimum value with an underestimation of 10–20% (Kochel et al., 1982, Baker, 1987, Enzel et al., 1993).

The two main assumptions for discharge calculation are 1) that significant aggradation and/or degradation of the channel has not occurred during the time-span of the flooding represented by the SWDs; and 2) that significant scour and/or fill in the river channel has not occurred during large flood events (Baker et al., 1983). For the study reach, both assumptions are acceptable because the river loops in sinuous curves of sandstone bedrock over a stable rock bed, which indicates very little bed change during the late Holocene (i.e. last three millennia).

3.4 Flood Frequency Analysis (FFA)

The annual maximum flood series and a partial duration flood series (PDS) were extracted from USGS gauge 09315000 on the Green River at Green River, Utah. There are 117 annual peak flows (1895-1899, 1905-2016, Figure. 2). However, only the unregulated annual maximum series (1895-1899, 1905-1961) is used, which closely represents the natural flow on the Green River. These 62 peaks were adjusted to the drainage area at the study site using the method of Cudworth (1989). It is assumed that the ratio of the peak discharges at the two locations is equal to the square root of their respective drainage areas, therefore the peak flows at the study sites are larger than the USGS gauge values by 4.9%. The largest seven paleoflood

peak flows were incorporated into the FFA by considering their extreme magnitudes and avoiding double-registration of the flood records. The largest paleoflood events (7500 m^3/s) takes the first place in FFA and assigned the oldest age (1330 Water Year). In this particular case the largest flood in the last 680 years is 7500 m3/s. The second largest event takes the second place with the second oldest age, and so on.

The FFA was conducted using HEC-SSP (Hydrologic Engineering Center's Statistical Software Package, v2.2) under the newly updated Guidelines for Determining Flood Flow Frequency Bulletin 17C (England, et al., 2018), which continues to fit the Log Pearson Type III (LP-III) distribution using the Expected Moments Algorithm (EMA) (Cohn et al., 1997, 2001; England et al., 2003, 2018) with the Multiple Grubbs-Beck test (MGBT) (Cohn et al., 2013; Lamontagne et al., 2013, 2015). EMA provides a direct fit of the LP-III distribution utilizing multiple types of at-site flood information including the systematic record, historical floods as well as paleofloods, while adjusting for any potentially influential low floods (PILF), missing values due to an incomplete record, or zero flood years.

We also employed the Bulletin 17B method (IACWD, 1982), the log normal distribution (Chow et al., 1988), the regional-regression equation (Kenney et al., 2007) and the self-similar model (Kidson and Richards, 2005; Malamud and Turcotte, 2006) with the systematic gauged peaks and the paleoflood data.

4 Results

4.1 Paleoflood slackwater deposits and chronology of the paleoflood events

Nine stratigraphic sequences of fine-grained flood deposits were found at the six study sites located along a 35-km long reach of Stillwater Canyon of the lower Green River (Figure 3).

Different slackwater depositional areas occurred in low-velocity flow environments during flooding, accumulating on stable rock platforms and alluvial terraces during flood recession. Suspended flood sediments were deposited, and eventually experienced long-term preservation in these regions. Characteristics of the slackwater depositional environments of the lower Green River paleoflood SWDs are summarized in Table 1.

Figure 5. Particle tracings and water depths associated with sites of DHC, PC, HB, and HD on the Lower Green River. Areas of slack-water deposition develop through combinations of flow direction, speed, and depth. For sites location see figure 3.

The 2D hydraulic model generated the paleoflood flow and velocity distributions in two dimensions, indicating the slackwater depositional zones (Figure 5). The SWDs at the Dead Horse Canyon site (DHC-1 and 2) are located in a low-velocity backwater area at the tributary mouth, while SWDs at the High Driftwood (HD) site is located on a high-velocity site at a >90 degrees curve where the sediments are probably super-elevated. The entire paleoflood record for the six sites consists of 68 paleoflood SWD layers and two driftwood lines at the HD site. These two driftwood lines are located 5 m and 12 m a.w.l. They are composed of coarse driftwood and logs. Since this is a multi-site record, it may well be that floods are presented at more than one site. The results of the AMS and OSL dating at the various sections indicate that all 70 units at six sites are deposited and preserved in 680-140 a (or 940-110 a bracketing the error), which can be represented by the RF-1 and DHC-1 sections (Figure 2). The OSL ages (550 -190 a) of 26 SWD layers at the RF-1 site cover all age ranges at the other five sites except for the DHC-1. The oldest unit at the DHC-1 section is 680 ± 250 a. At least 27 paleoflood events are therefore considered to have occurred in the past 680 years (Table 2 and 3).

4.2 Paleoflood hydrodynamics

The 2D hydraulic model was run for approximately 12 different discharge levels at each SWD site. These levels ranged upward from 50 m^3/s, which is a flow just large enough to begin submerging the lowest SWDs at the six sites. Rating curves were then fitted based on the stimulated discharge-stage (Q-S) points following the equation:

$$\boldsymbol{Q = C(h - e)^{\beta}},$$

where Q is the stimulated flow discharge for a certain height of the water surface, m^3/s; h is the height of the water surface, m; e is the height of the lowest point of a cross-section, m; (h – e) is head or water depth, m. C, and β are calibration coefficients. C indicates flow discharge when water depth (h – e) is equal to 1; and β is the slope of the rating curve.

Water dynamic conditions are represented in the model output by particle tracings and water depth near each SWD site on the study reach (Figure 5). The paleoflood peak discharges were estimated using the rating curve equations combined with the relevant water stages (Figure 6 and Table 4). All the paleoflood peaks ranged between -20.4% and 7.2% when the Manning's n value was adjusted by ±25% (Figure 6 and Table 4). The largest magnitude of paleoflood was about 7500 m^3/s (-9.2-3.0%) with a water stage of 13.50 meters above the river water level. There are at least 14 paleofloods with magnitudes larger than twice the maximum systematic gauged record of 1929 m^3/s.

Figure 6. Rating curves (solid lines) and corresponding results (dashed lines) for the 25% of Manning's n variation for six cross sections at the paleoflood sites on the Lower Green River. The sensitivity test shows an error of 3.0-20.4% can be introduced by the uncertainty of Manning's n.

4.3 Flood Frequency Analysis (FFA)

The results of FFA based on various methods and flood series are shown in Figures 7-9 and Table 5-7. For the Bulletin 17C method, the annual peak flows including the systematic record and paleofloods are all described by flow interval ($Q_{Y,lower}$, $Q_{Y,upper}$) and perception thresholds ($T_{Y,lower}$, $T_{Y,upper}$) in Figure 7 and Table 5-6. •The perception thresholds ($T_{Y,lower}$, $T_{Y,upper}$) are used describe the sample properties in EMA. They describe the range of measurable potential discharges and are independent of the actual peak discharges that have occurred. The lower perception threshold ($T_{Y,lower}$) represents the smallest peak that have happened. In this study, $T_{Y,lower}$ for each event is the minimum estimated discharge for that event. $T_{Y,upper}$ is assumed to be infinite, as bigger floods that might exceed known highwater marks and other physical evidence of the flood. The station skew was used in this study. Expected quantiles for the interval floods are shown with 95% confidence limit in Figure 7a and b. Combining both the paleoflood data and systematic peaks, the FFA shows the largest paleoflood (7500 m^3/s) has an AEP (annual exceedance probability) of 0.057% or a return period of 1750 years, while the AEP and return period for the largest gauged flood (2023 m^3/s) are 3.770% and 26.5 years (Fig. 8a). In contrast, the FFA using only the systematic peaks shows that the return period for the largest paleoflood is longer than 1,000,000 years, for the largest gauged flood 68.5 years (Fig. 8b). The ratio of 95% confidence interval to the expected quantile (CI/EQ) is used to illustrate the effects of change with the integration of paleoflood data (Fig. 8c). Paleofloods increased both the expected quantiles and confidence intervals of the 25-year-flood and the longer recurrence interval floods to various extents, while the CI/EQ was reduced by 20% for 25-year-flood, 27% for 50-year-flood, 24% for 100-year-flood, and 17% for 200-year-flood.

Figure 7. Graph showing approximate systematic peak discharge and paleoflood estimates, with paleoflood exceedance thresholds, on the Lower Green River in the Stillwater Canyon reach. A

scale break is used to separate the gaging station data from the much longer paleoflood record. Flood intervals for large floods in the paleoflood period are shown as red squares and black vertical bars with caps that represent minimum peaks and an additional 20% of the minimum. Mean values of paleofloods threshold age data are plotted for simplicity. Perception threshold ranges are shown as orange lines for the paleoflood period, blue lines for the systematic period, and green lines for the discontinued period. The gray shaded areas represents: (1) floods of unknown magnitude less than the perception thresholds for the paleoflood periods Tp,lower ; (2) the discontinued period Td,lower; (3) post-regulation floods after 1961.

Figure 8. Results of flood frequency analysis (FFA) using Expected Moments Algorithm (EMA) with Multiple Grubbs-Beck Test (MGBT) on the Lower Green River in the Stillwater Canyon reach, using (a) both systematic and paleoflood data; (b) systematic peaks only. The solid line is the fitted log-Pearson Type III frequency curve and the dash lines are the 95% confidence limits. Peak discharge estimates from the gauge are shown as open circles; vertical bars represent estimated data uncertainty for paleofloods; the solid black circle is the potentially influential low flood (PILF) threshold as identified by the MGBT. Y-axis of the subplot (c), CI/EQ, is the ratio of confidence limits to expected quantiles.

Figure 9. Comparison of different techniques for flood frequency analysis (FFA) on the Lower Green River in the Stillwater Canyon reach, including systematic and paleoflood data. Subplots a-e include nine FFA curves using five techniques and all of them were synthesized in the subplot f. Annual exceedance probability (AEP), return period (T), and discharge (Q) for these curves

are summarized in Table 7. The numbers refer to the discussion of each curve in the text and table.

Other flood probability models also showed a good fit with most data points (Fig. 9). Curves 1, 3, 5, 7 were calculated using the Bulletin 17C, Bulletin 17B methods, a log-normal distribution, and the self-similar model, combining paleoflood data with the systematic annual maximum flood series (except that the partial duration flood series was used for the self-similar model). Curves 2, 4, 6, 8 were calculated using the same approaches, but with only the systematic peaks. Curve 9 employed the regional-regression equation. Relatively good agreement is observed among the different FFA techniques for recurrence intervals of less than ten years. Two clusters appeared with increasing recurrence intervals. Curves 1, 3, 5, 7, and 8 occupied the first cluster, showing high upper tails. The low values were estimated by curves 2, 4, 6, and 9, which are limited to analysis of only the systematic peaks. Clearly, the paleoflood data swing up the upper tails for the log P-III and lognormal distributions (Fig. 8a, b, and c). However, curves 7 and 8 demonstrated that the expected quantiles correspond very closely with a power-law distribution for recurrence interval larger than 25 years; they both were in good agreement with paleoflood involved Bulletin 17C results (curve 1).

5 Discussion and Conclusions

The protection against extreme floods for large, high-hazard, water-related projects and engineered systems, including high-level dams and nuclear power plants, is a long-standing hydrological issue. Hydrologists developed two primary procedures for flood-protection decision-making: (1) FFA, based on the statistical analysis of peak flood distributions, and (2) probable maximum flood (PMF) calculations. Despite inherent difficulties and controversies involving both methods, emerging since the 1960s (e.g., Yevjevich, 1968) or earlier, both

procedures have, nevertheless, been applied extensively and established either as engineering standards or official guidance in the United States and many other countries (Hydrology Committee, U.S W.R.C., 1977; National Environment Research Council, 1999; SL44-2006).

It has now been more than a century, since 1914, when the concept of a return period of a flood event of a given magnitude or average recurrence interval was proposed by Fuller (1914), and statistical techniques were introduced for the hydrological analysis of flood extremes. Early on this procedure was known to require a sufficiently large number of flood events for statistical validity such that the parameters met the requirement of being, independent, identically-distributed random variables (Kisiel, 1969). These requirements reflect fundamental assumptions necessary for FFA that a specific magnitude of flood corresponds to a specific probability or return period. The objective of FFA is to find this relationship, especially to predict the upper tails for the relevant distributions (Klemeš, 2000). However, it is almost always, not possible to collect statistically large enough samples to validly estimate the greatest extremes, even in the U.S. where the hydrological gauging network has been established since late 19th century (U.S. Water Resources Council, 1988). The gauged data are always restricted to samples overwhelming dominated by small and common floods, whereas data on extremely large, rare floods are not captured in the instrumental data, making this assumption inadequate for making valid statistical inferences. This circumstance inevitably leads to extrapolation from the existing gauged data.

The incorporation of paleoflood data into FFA started in the late 1970s (Costa, 1978; Baker et al., 1979). In a seminal study Stedinger and Cohn (1986) examined three methods for utilizing paleoflood information in flood-frequency analysis (see also Stedinger and Baker, 1987). Cohn et al. (1997) developed a method of expected moments algorithm (EMA) for

utilizing paleoflood information in FFA, and this procedure has become the basis for the newly published Bulletin 17C (England, et al., 2018). Frances (2001) showed how to include paleoflood data in FFA using the Maximum Likelihood Estimation (MLE) method. Lam et al. (2017) integrated paleoflood data into FFA using Bayesian Inference methods, thereby showing a significant reduction in uncertainty for 100-yr flood estimation in subtropical Australia. Multiple studies have focused on assessing the contribution of PFH to FFA improvement by promoting the incorporation of paleoflood data. In these many studies, the utilization of paleoflood information for FFA simply enriches the flood samples for the statistical manipulation. As Klemeš (1987, 1994) strongly asserted, "… much of FFA is just a part of small sample theory in disguise, the term 'flood' being used merely as a name for numbers employed."

PMF estimation employs both meteorological and hydrological approaches to calculate the theoretically maximum flood for a basin of interest (WMO, 2009). The PMF for a given basin is derived from the probable maximum precipitation (PMP), which is defined by American Meteorological Society as, "…the theoretically greatest depth of precipitation for a given duration, that is physically possible over a particular drainage at a certain time of the year." This means the PMF method must assume that there is a natural upper limit to precipitation for a given duration and area. Based on this assumption, the PMF can then be estimated to an upper limit of flood magnitude by hydrological modeling that incorporates the most extreme combination of hydrological conditions. However, it is difficult, if not impossible for the reality of a changing world, to establish the validity of any assumed upper limit to either precipitation or flooding. The established methods for PMP/PMF estimation are, necessarily based on known, limited observations and the current state of knowledge, specific to the circumstances of time and place. However, in the real world both data and the intelligence with which to understand

things, i.e., science, are increasing (Jakob et al., 2009; Song et al., 2015). PMP/PMF estimates are consequently observed to increase as more sophisticated meteorological phenomena observed and recognized (Kunkel, 2013). Moreover, the magnitude of PMP/PMF can also vary widely by using different methods (Douglas and Barros, 2003; Jakob et al., 2009; Rouhani and Leconte, 2016). The hydrological model transforming the PMP into PMF uses a science-as-knowledge approach, of which it underpins valid reasoning about what can be said to the world. The extreme floods generated by a hydrological model are therefore, considered as what we human created, rather than what really happened in nature. The most controversial observation is that PMP/PMF values have been exceeded by actual extreme events (Bewsher & Maddocks, 2003). A relevant example is the recent discovery of two naturally-evidenced extreme floods, i.e., paleofloods, occurring in the last 2000 years, and found to be larger than the PMF for the upper Colorado River (Greenbaum et al., 2014).

This review of problems and criticisms of both the FFA and PMF methodologies raises even more fundamental concerns about the epistemological underpinnings in regard to the scientific understanding of the nature of extreme floods. While these are not usually issues considered in the practical expediency necessary to achieve engineering solutions, they do emerge when phenomena are at the limits of scientific understanding. Extreme flooding lies at those limits. Both the FFA and PMF methods employ theory-directed, science-as-knowledge approaches, which hold the world to be a system that permits the application of deductive logic through mathematics to provide the certainty associated with that kind of reasoning (Baker, 2017). But that certainty only applies if the assumptions made are absolutely true.

In this study, state-of-the-art paleoflood hydrology (PFH) was applied to provide information on extreme floods not captured in the short instrumental record. PFH derives from a

science-as-seeking point of view and employs a world-directed, investigative approach (Baker, 2017) to discover the extreme floods that have actually happened over a geological span of time (commonly limited to the Holocene epoch, a period about the last 11,700 years, characterized by Earth's non-glacial climate regimes). PFH thereby provides reliable, fundamental knowledge concerning extreme flood behavior in nature. It thus makes previously unknown extreme floods known to appropriately experienced investigators, thereby revealing what would otherwise be hidden within hydrological assumptions. By directly compiling evidence from the world, in a sense listening to the nature what nature presents to us, and thinking based on realities, PFH investigators study the clues, signals, and signs of the most extreme floods found in nature. In following these signs, an explanatory working hypothesis emerges as to what is actually possible, and every inference to what is probable must also infer what is possible. This is abductive inference (Baker, 2017) and the associated natural historical approach yields real-world discoveries about extreme floods, which form the basis for advancing scientific understanding about such flooding.

By employing paleoflood hydrological investigation, this study identified at least 27 real extreme floods that occurred on the lower Green River during the last 700 years. Combining the water stages inferred by the tops of paleoflood SWD layers, the 2D hydraulic modeling retrodicted the minimum peak paleo-discharges at six study reaches. Among them at least 14 paleofloods were larger than twice of the maximum systematic gauged record of 1929 m^3/s. The largest paleoflood has a minimum peak discharge of 7500 m^3/s.

These numbers more accurately reflect the actual history of extreme floods on the Green River, rather than either (1) the extrapolated ones from small-scale flood samples, or (2) the derived outputs from a hydrological (watershed) model. This is unlike both conventional FFA or

the hydrological rainfall-runoff models used for PMF estimation, which respectively, involve either generating probabilistically extrapolated upper tails or the deterministically deduce limiting upper values via models and assumptions, providing the established practical tools for predicting extreme floods in flood mitigation projects or design flood estimations (U.S. Army Corps of Engineers, 1991; U.S. Bureau of Reclamation, 2003). However, these practical tools can only be claimed to be science-based if their predictions are compared to the information nature provides to us about extreme flood events, i.e., there is agreement with empirical evidence—not just empirical evidence that is convenient in the artificial repositories of our existing data sets, but all possible empirical evidence, which includes that being held by nature itself in its natural repositories. To ignore realities is to be "unscientific." PFH continues the exploratory imperative of what is most essential in a doing science of extreme flooding by making discoveries of viable and efficient data sources from real-world evidence, which can act as a "spotlight" for improving both FFA (Schendel and Thongwichian, 2017; Lam et al., 2017) and hydrological modeling (England et al., 2014) of extreme floods.

Finally, it can be observed that the clustering of paleoflood patterns offers an opportunity to explore complex, spatially highly interrelated flood-climate links in a global perspective (Baker, 1987; 2008; Ely et al., 1993; Hischboeck et al., 1988; Knox, 2000;; Macklin, 2006; Merz et al., 2014; Benito et al., 2015; Toonen et al., 2017), which, combined with other information on paleoclimates, can provide valuable insights into understanding the nature of extreme floods (Merz et al., 2014). Ely et al. (1993; 1997) displays the clustered extreme paleofloods in the last 4000 years in the southwestern U.S. and identified the hydroclimatic effect on the increased flood frequency. Harden et al. (2010) also suggests that hydroclimatic dynamics strongly affected the episodes of major flood events during the Holocene based on a broader paleoflood

dataset for the southwestern U.S. The results of this study agree with previous research (Ely et al., 1993; Harden et al., 2010; Greenbaum et al., 2014) that frequent large floods happened during periods of cool and dry climate. Knox (1993, 2000) highlighted that significant changes in magnitudes and frequencies of extreme paleofloods are regional hydrological responses to global climatic change. Huang et al. (2007, 2010) and Liu et al. (2014) inferred that major Holocene flood episodes are associated with transitional periods of climatic change, forced by monsoonal shifts in northern and central China. Benito et al. (2015) examined the relationship between Holocene flood patterns and short-term climatic variability in Europe and North Africa, suggesting the importance of paleoflood information for understanding future spatial-temporal changes of flood frequency. Toonen et al. (2017) implied that individual flood events and multiyear episodes generally fall within extended flood-rich phases controlled by climate, demonstrating the value of paleoflood datasets as useful multiscale hydromorphic signals of climate change. Recent studies (Munoz et al., 2017 and 2018) suggest that El Niño increase the risk of Mississippi flooding and conventional flood prediction techniques-based engineering control measures might actually be making floods worse.

Much remains for research in the future, but the only resource and basis we can rely on is to find out what's naturally true of extreme floods is the history of past manifestations. It cannot be overemphasized that a truly scientific understanding of extreme floods can only emerge from our exploration in nature of flood signs in all their temporal contexts (paleo-, historical, and systematically gauged), to be followed by the explanation of the discovered (not presumed) phenomena through a mechanistic understanding of their causal drivers.

Acknowledgments

This research was supported by the U.S. Bureau of Reclamation under Assistance Agreement no. R16AC00021. V.R.B.'s 45-year program of developing paleoflood hydrological science received critical early support from the U.S. National Science Foundation. This paper is Contribution Number 105 of the Arizona Laboratory of Paleohydrological and Hydroclimatological Analysis (ALPHA).

References

Aitken, M.J. 1998: An Introduction to Optical Dating: The dating of Quaternary sediments by the use of photon-stimulated luminescence. New York, Oxford University Press, 267 p.

Aitken, M.J., Xie, J., 1990. Moisture correction for annual gamma dose. Ancient TL 8 (2), 6-9.

Baker, V. R., Kochel, R. C., Patton, P. C., and Pickup, G.: 1983, Paleohydrologic analysis of Holocene flood slack-water sediments, Internat. Assoc. of Sedimentologists Special Publ. 6, 229–239.

Baker, V.R., 1975. Flood hazards along the Balcones Escarpment in central Texas: alternative approaches to their recognition, mapping and management. University of Texas Bureau of Economic Geology Circular, vol. 75–5. 22 pp.

Baker, V.R., 1987. Paleoflood hydrology and extraordinary flood events. J. Hydrol. https://doi.org/10.1016/0022-1694(87)90145-4

Baker, V.R., 1996, Discovering the future in the past: Palaeohydrology and geomorphological change, in Branson, J., Brown, A.G., and Gregory, K.T., editors, Global continental changes: The context of palaeohydrology: The Geological Society of London, Special Publication No. 115, p. 73-83.

Baker, V.R., 1998, Paleohydrology and the hydrological sciences, in Benito, G., Baker, V.R., and Gregory, K.J., editors, Palaeohydrology and environmental change: John Wiley and Sons, Chichester, p. 1-10.

Baker, V.R., 2008. Paleoflood hydrology: Origin, progress, prospects. Geomorphology 101, 1–13. https://doi.org/10.1016/J.GEOMORPH.2008.05.016

Baker, V.R., 2013. Global Late Quaternary Fluvial Paleohydrology: With Special Emphasis on Paleofloods and Megafloods, in: John F. Shroder (Ed.), Treatise on Geomorphology. Academic Press, San Diego, pp. 511–527.

Baker, V.R., 2017. Debates-Hypothesis Testing in Hydrology: Versus Pursuing Uberty. Water Resour. Res. 53, 1770–1778. https://doi.org/10.1002/2016WR020078.

Baker, V.R., Kochel, R.C., Patton, P.C., 1979. Long-term flood frequency analysis using geological data. Int. Assoc. Hydrol. Sci. 128, 3–9.

Baker, V.R., Kochel, R.C., Patton, P.C., Pickup, G., 1983. Palaeohydrologic analysis of Holocene flood slack-water sediments., in: Collinson, J.D., Lewin, J. (Eds.), Modern and Ancient Fluvial Systems. Blackwell Scientific; International Association of Sedimentologists, Special Publication 6, pp. 229–239.

Baker, V.R., Pickup, G., Polach, H.A., 1985. Radiocarbon dating of flood events, Katherine Gorge, Northern Territory, Australia. Geology 13, 344–347. https://doi.org/10.1130/0091-7613(1985)13<344:RDOFEK>2.0.CO;2

Baker, V.R., Webb, R.H., House, P.K., 2002. The scientific and societal value of paleoflood hydrology. In: House, P.K., Webb, R.H., Baker, V.R., Levish, D.R. (Eds.), Ancient Floods, Modern Hazards: Principles and Applications of Paleoflood Hydrology. Water

Science and Application, vol. 5. American Geophysical Union,Washington, D.C., pp. 1–19.

Benito, G., Macklin, M.G., Panin, A., et al., 2015. Recurring flood distribution patterns related to short-term Holocene climatic variability. Sci. Rep. 5, 1–8. https://doi.org/10.1038/srep16398

Benito, G., O'Connor, J.E., 2013. Quantitative Paleoflood Hydrology, in: Shroder, J. (Editor in Chief), Wohl, E. (Ed.), Treatise on Geomorphology. Academic Press, San Diego, pp. 459–474. https://doi.org/10.1016/B978-0-12-374739-6.00250-5

Benito, G., Sopeña, A., Sánchez-Moya, Y., Machado, M.J., Pérez-González, A., 2003. Palaeoflood record of the Tagus River (Central Spain) during the Late Pleistocene and Holocene. Quat. Sci. Rev. 22, 1737–1756. https://doi.org/10.1016/S0277-3791(03)00133-1

Blinn, Dean W., Poff, N.L., 2005. Colorado River Basin, in: Arthur C. Benke (Ed.), Rivers of North America. Academic Press, pp. 482–538. https://doi.org/10.1016/B978-012088253-3/50014-6

Brown, S.L., Bierman, P.R., Lini, A., Southon, J., 2000. 10 000 yr record of extreme hydrologic events. Geology 28, 335–338. https://doi.org/10.1130/0091-7613(2000)28<335:YROEHE>2.0.CO;2

Cashion, W.B., 1967. Geology and fuel resources , of the Green River Formation southeastern Uinta basin Utah and Colorado. U.S. Geol. Surv. Prof. Pap. 548 48.

Centre for Ecology & Hydrology.

Chow, V.T., Maidment, D.R. and Mays, L.W., 1988. Applied Hydrology, 1st ed. McGraw-Hill Book Company, New York.

Cohn, T.A., Lane, W.L., Baier, W.G., 1997. An algorithm for computing moments- based flood quantile estimates when historical flood information is available. Water Resour. Res. 33, 2089–2096. https://doi.org/10.1029/97WR01640

Costa, J.E., 1978. Holocene stratigraphy in flood frequency analysis. Water Resour. Res. 14, 626–632. https://doi.org/10.1029/WR014i004p00626

Costa, J.E., 1978. Holocene stratigraphy in flood-frequency research. Water Resources Research 14, 626–632.

Cudworth, A.G., 1989. Flood Hydrology Manual: A Water Resources Technical Publication, 1st ed, United States Department of the Interior Bureau of Reclamation, Denver.

Douglas, E.M., Barros, A.P., 2003. Probable maximum precipitation estimation using multifractals: Application in the eastern United States. J. Hydrometeorol. 4, 1012–1024. https://doi.org/10.1175/1525-7541(2003)004<1012:PMPEUM>2.0.CO;2

Ely, L.L., 1997. Response of extreme floods in the southwestern United States to climatic variations in the late Holocene. Geomorphology 19, 175–201. https://doi.org/10.1016/S0169-555X(97)00014-7

Ely, L.L., Baker, V.R., 1985. Reconstructing paleoflood hydrology with slackwater deposits: Verde River, Arizona. Phys. Geogr. 6, 103–126. https://doi.org/10.1080/02723646.1985.10642266

Ely, L.L., Enzel, Y., Baker, V.R., Cayan, D.R., 1993. A 5000-year record of extreme floods and climate change in the Southwestern United States. Science. 262, 410–412. https://doi.org/https://www.jstor.org/stable/2883155

England, J.F., Godaire, J.E., Klinger, R.E., Bauer, T.R., Julien, P.Y., 2010. Paleohydrologic bounds and extreme flood frequency of the Upper Arkansas River, Colorado, USA. Geomorphology 124, 1–16. https://doi.org/10.1016/j.geomorph.2010.07.021

England, J.F. Jr., Julien, P.Y., and Velleux, M.L., 2014. Physically-Based Extreme Flood Frequency Analysis using Stochastic Storm Transposition and Paleoflood Data on Large Watersheds, J. Hydrol., 510, doi:10.1016/j.jhydrol.2013.12.021, pp. 228-245.

England, J.F., Jr., Cohn,T.A., Faber,B.A., Stedinger, J.R., Thomas, W.O., Jr., Veilleux, A.G., Kiang, J.E., and Mason, R.R., Jr., 2018, Guidelines for determining flood flow frequency—Bulletin 17C: U.S. Geological Survey Techniques and Methods, book4, chap. B5, 148p., .

Enzel, Y., Ely, L.L., House, P.K., Baker, V.R., Webb, R.H., 1993. Paleoflood evidence for a natural upper bound to flood magnitudes in the Colorado River Basin. Water Resour. Res. 29, 2287–2297. https://doi.org/10.1029/93WR00411

Enzel, Y., Ely, L.L., Martinez-Goytre, J., Vivian, R.G., 1994. Paleofloods and a dam-failure flood on the Virgin River, Utah and Arizona. J. Hydrol. 153, 291–315. https://doi.org/https://doi.org/10.1016/0022-1694(94)90196-1

Francés, F., 2001. Incorporating Non-Systematic Information to Flood Frequency Analysis Using the Maximum Likelihood Estimation Method, in: Glade, T., Albini, P., Francés,

Félix (Eds.), The Use of Historical Data in Natural Hazard Assessments. Springer Netherlands, Dordrecht, pp. 89–99. https://doi.org/10.1007/978-94-017-3490-5_7

Fuller, J.E. 1987. Paleoflood hydrology of the alluvial Salt River, Tempe, Arizona. M.S. thesis, University of Arizona, Tucson.

Fuller, W. E. (1914). Flood flows. Transactions of the American Society of Civil Engineers, LXXVII(1), 564–618.

Greenbaum, N., A. Ben-Zvi, I. Haviv, Y. Enzel, 2006. T hydrology and paleohydrology of the Dead Sea tributaries. In: Y. Enzel, A. Agnon, M. Stein (Eds.), New Frontiers in Dead Sea Paleoenvironmental Research, Geological Society of America, Special Paper 401, p. 63-94.

Greenbaum, N., Schick, A.P., Baker, V.R., 2000. The paleoflood record a hyperarid catchment, Nahal Zin, Negev Desert, Israel. Earth Surface Processes and Landforms 25, 951–971.

Greenbaum, Noam; Harden, Tessa M.; Baker, V.R., Weisheit, J., Cline, M.L., Porat, N., Halevi, R., Dohrenwend, J., 2014. A 2000 year natural record of magnitudes and frequencies for the largest Upper Colorado River floods near Moab, Utah. Water Resour. Res. 50, 1–21. https://doi.org/10.1002/2013WR014835.Received

Guérin, G., Mercier, N., Adamiec, G., 2011. Dose-rate conversion factors: update: Ancient TL 29, 5-8.

Harden, T., Macklin, M.G., Baker, V.R., 2010. Holocene flood histories in south-western USA. Earth Surf. Process. Landforms 35, 707–716. https://doi.org/10.1002/esp.1983

Hirschboeck KK. 1988. Flood hydroclimatology. In Flood Geomorphology, Baker VR, Kochel RC, Patton PC (eds). John Wiley and Sons: New York; 27–49.

House, P.K., Webb, R.H., Baker, V.R., Levish, D. (Eds.), 2002. Ancient Floods, Modern Hazards: Principles and Applications of Paleoflood Hydrology. Water Science and Application, vol. 5. American Geophysical Union. 385 pp.

Huang, C.C., Pang, J., Zha, X., Zhou, Y., Su, H., Li, Y., 2010. Extraordinary Floods of 4100−4000 a BP recorded at the Late Neolithic Ruins in the Jinghe River Gorges, Middle Reach of the Yellow River, China. Palaeogeogr. Palaeoclimatol. Palaeoecol. 289, 1–9. https://doi.org/10.1016/J.PALAEO.2010.02.003

Huang, C.C., Pang, J., Zha, X., Su, H., Jia, Y., Zhu, Y., 2007. Impact of monsoonal climatic change on Holocene overbank flooding along Sushui River, middle reach of the Yellow River, China. Quat. Sci. Rev. 26, 2247–2264. https://doi.org/10.1016/J.QUASCIREV.2007.06.006

Hydrology Committee, U.S W.R.C., 1977. Guidelines for determining flood flow frequency, 1977. Washington: Water Resources Council, Hydrology Committee.

IACWD, 1982. Guidelines for determining flood flow frequency, Bulletin 17-B. Technical report, Interagency Committee on Water Data, Hydrology Subcommittee.

Institute of Hydrology, 1999. Flood Estimation Handbook (five volumes). Wallingford:

Jakob, D., Smalley, R., Meighen, et al., 2009. Climate change and probable maximum precipitation. Melbourne: Bureau of Meteorology, Australian Government, Hydrometeorological Advisory Service, Water Division.

Jarrett, R.D., 1990. Paleohydrologic techniques used to define the spatial occurrence of floods. Geomorphology 3, 181–195. https://doi.org/10.1016/0169-555X(90)90044-Q

Jones, A.., Shimazu, H., Oguchi, T., Okuno, M., Tokutake, M., 2001. Late Holocene slackwater deposits on the Nakagawa River, Tochigi Prefecture, Japan. Geomorphology 39, 39–51. https://doi.org/10.1016/S0169-555X(01)00050-2

Kale, V.S., Mishra, S., and Baker, V.R., 1997, A 2000-year palaeoflood record from Sakarghat on Narmada, central India: Journal of the Geological Society of India, 50, 283-288.

Kenney, T.A., Wilkowske, C.D., Wright, S.J., 2008. Methods for Estimating Magnitude and Frequency of Peak Flows for Natural Streams in Utah. U.S. Geol. Surv. Sci. Investig. Rep. 2007–5158, 28.

Kidson, R., Richards, K.S., 2005. Flood frequency analysis: Assumptions and alternatives. Prog. Phys. Geogr. 29, 392–410. https://doi.org/10.1191/0309133305pp454ra

Kiseiel, C.C., 1969. Time Series Analysis of Hydrologic Data. Adv. Hydrosci. 5, 1–119. https://doi.org/10.1016/B978-1-4831-9936-8.50007-6

Klemeš, V., 1987. Hydrological and engineering relevance of flood frequency analysis, in: Singh, V.P. (Ed.), Hydrologic Frequency Modeling. D. Reidel Publishing Co., Dordrecht, pp. 1–18.

Klemeš, V., 2000. Tall Tales about Tails of Hydrological Distributions. I. J. Hydrol. Eng. 5, 227–231. https://doi.org/10.1061/(ASCE)1084-0699(2000)5

Klemeš, V., 1994. Statistics and probability: Wrong remedies for a confused hydrologic modeler, in: Barnett, V., Turkman, K.F. (Eds.), Statistics for the Environment 2. John Wiley and Sons, London, pp. 345–366.

Knox, J.C., 1985. Responses of floods to Holocene climatic change in the upper Mississippi Valley. Quat. Res. 23, 287–300. https://doi.org/10.1016/0033-5894(85)90036-5

Knox, J.C., 1993. Large increases in flood magnitude in response to modest changes in climate. Nature 361, 430–432. https://doi.org/10.1038/361430a0

Knox, J.C., 2000. Sensitivity of modern and Holocene floods to climate change. Quat. Sci. Rev. 19, 439–457. https://doi.org/10.1016/S0277-3791(99)00074-8

Kochel, R.C., Baker, V., 1988. Paleoflood analysis using slackwater deposits, in: Baker, V.R., Kochel, R.C., Patton, P.C. (Eds.), Flood Geomorphology. Wiley, New York, pp. 357–376.

Kochel, R.C., Baker, V.R., Patton, P.C., 1982. Paleohydrology of southwestern Texas. Water Resour. Res. 18, 1165–1183. https://doi.org/10.1029/WR018i004p01165

Kunkel, K.E., Karl, T.R., Easterling, D.R., Redmond, K., Young, J., Yin, X., Hennon, P., 2013. Probable maximum precipitation and climate change. Geophys. Res. Lett. 40, 1402–1408. https://doi.org/10.1002/grl.50334

Lai, Y.G., 2010. Two-dimensional depth-averaged flow modeling with an unstructured hybrid mesh. J. Hydraul. Eng. 136, 12–23. https://doi.org/10.1061/(ASCE)HY.1943-7900.0000134

Lam, D., Thompson, C., Croke, J., Sharma, A., Macklin, M., 2017. Reducing uncertainty with flood frequency analysis: The contribution of paleoflood and historical flood information. Water Resour. Res. 53, 2312–2327. https://doi.org/10.1002/2016WR019959

Liu, T., Huang, C.C., Pang, J., Zhou, Y., Zhang, Y., Ji, L., Shang, R., 2014. Extraordinary hydro-climatic events during 1800–1600 yr BP in the Jin–Shaan Gorges along the middle Yellow River, China. Palaeogeogr. Palaeoclimatol. Palaeoecol. 410, 143–152. https://doi.org/10.1016/J.PALAEO.2014.05.039

Macklin, M.G., Benito, G., Gregory, K.J., et al., 2006. Past hydrological events reflected in the Holocene fluvial record of Europe. Catena. https://doi.org/10.1016/j.catena.2005.07.015

Malamud, B.D., Turcotte, D.L., 2006. The applicability of power-law frequency statistics to floods. J. Hydrol. 322, 168–180. https://doi.org/10.1016/J.JHYDROL.2005.02.032

Merz, B., Aerts, J., Arnbjerg-Nielsen, K., et al., 2014. Floods and climate: Emerging perspectives for flood risk assessment and management. Nat. Hazards Earth Syst. Sci. 14, 1921–1942. https://doi.org/10.5194/nhess-14-1921-2014

Munoz, S. E. and Dee, S. G., 2017. El Niño increases the risk of lower Mississippi River flooding. Sci. Rep. 7, https://doi.org/10.1038/s41598-017-01919-6.

Munoz, S.E., Giosan, L., Therrell, M.D., Remo, J.W.F., Shen, Z., Sullivan, R.M., Wiman, C., O'Donnell, M., Donnelly, J.P., 2018. Climatic control of Mississippi River flood hazard amplified by river engineering. Nature 556, 95–98. https://doi.org/10.1038/nature26145

Murray, A.S., Wintle, A.G., 2000. Luminescence dating of quartz using an improved single-aliquot regenerative-dose protocol. Radiat. Meas. 32, 57–73. https://doi.org/10.1016/S1350-4487(99)00253-X

Murray, A.S., Wintle, A.G., 2003. The single aliquot regenerative dose protocol: potential for improvements in reliability. Radiat. Meas. 37, 377–381. https://doi.org/10.1016/S1350-4487(03)00053-2

National Environment Research Council, 1999: Flood Studies Report, (in five volumes) Wallingford: Institute of Hydrology.

National Research Council, 1988. Estimating probabilities of extreme floods: methods and recommended research. The National Academy Press, Washington, DC. https://doi.org/10.17226/18935

O'Connor, J.E., Curran, J.H., Beebee, R.A., Grant, G.E., Sarna-Wojcicki, A., 2003. Quaternary Geology and Geomorphology of the Lower Deschutes River Canyon, Oregon. Oregon Water Sci. Appl. 7, 77–98.

O'Connor, J.E., Ely, L.L., Wohl, E.E., et al., 1994. A 4500-year record of large floods on the Colorado River in the Grand Canyon, Arizona. J. Geol. 102, 1–9. https://doi.org/https://www.jstor.org/stable/30065707

Ostenaa, D.A., Levish, D.R., O'Connell, D.R.H., 1996. Paleoflood study for Bradbury Dam, Cachuma Project, California. U.S. Bureau of Reclamation Seismotectonic Report 96-3, Denver, CO.

Partridge, J., Baker, V.R., 1987. Palaeoflood hydrology of the Salt river, Arizona. Earth Surf. Process. Landforms 12, 109–125. https://doi.org/10.1002/esp.3290120202

Patton, P.C., Baker, V., 1977. Geomorphic response of central Texas stream channels to catastrophic rainfall and runoff., in: Doehring, D.O. (Ed.), Geomorphology in Arid Regions. Proc. 8th Binghamton Symposium in Geomorphology, 1977. Allen & Unwin, pp. 189–217.

Patton, P.C., Dibble, D.S., 1982. Archaeologic and geomorphic evidence for the paleohydrologic record of the Pecos River in west Texas. Am. J. Sci. 282, 97–121. https://doi.org/10.2475/ajs.282.2.97

Pickup, G., Allan, G., Baker, V.R., 1988. History, palaeochannels and palaeofloods of the Finke River, central Australia, in: Warner, R.F. (Ed.), Fluvial Geomorphology of Australia. Academic Press, pp. 177–200.

Prescott, J.R., Hutton, J.T., 1994. Cosmic ray contributions to dose rates for luminescence and ESR dating: Large depths and long-term time variations. Radiat. Meas. 23, 497–500. https://doi.org/10.1016/1350-4487(94)90086-8

Rouhani, H., Leconte, R., 2016. A novel method to estimate the maximization ratio of the Probable Maximum Precipitation (PMP) using regional climate model output. Water Resour. Res. 52, 7347–7365. https://doi.org/10.1002/2016WR018603

Saint-Laurent, D., Couture, C., McNeil, É., Baudouin, Y., 2001. Spatio-temporal analysis of floods of the Saint-François drainage basin, Québec, Canada. Canada Environ. 29, 73–89.

Sheffer, N.A., Enzel, Y., Benito, G., Grodek, T., Poart, N., Lang, M., Naulet, R., Cœur, D., 2003. Paleofloods and historical floods of the Ardèche River, France. Water Resour. Res. 39. https://doi.org/10.1029/2003WR002468

SL44-2006, 2006. Regulation for calculating design flood of water resources and hydropower projects, Ministry of Water Resources, P.R. China. China Water&Power Press, Beijing: 1-92.

Song, X., Song, S., Sun, W., Mu, X., Wang, S., Li, J., Li, Y., 2015. Recent changes in extreme precipitation and drought over the Songhua River Basin, China, during 1960–2013. Atmos. Res. 157, 137–152. https://doi.org/10.1016/J.ATMOSRES.2015.01.022

Springer, G.S., Kite, J.S., 1997. River-derived slackwater sediments in caves along Cheat River, West Virginia. Geomorphology 18, 91–100. https://doi.org/10.1016/S0169-555X(96)00022-0

Stedinger, J.R., Baker, V.R., 1987. Surface water hydrology: historical and paleo-flood information. Rev. Geophys. 25, 119–124.

Stedinger, J.R., Cohn, T.A., 1986. Flood Frequency Analysis With Historical and Paleoflood Information. Water Resour. Res. 22, 785–793. https://doi.org/10.1029/WR022i005p00785

Stedinger, J.R., Griffis, V.W., 2008. Flood Frequency Analysis in the United States: Time to Update. Journal of Hydrologic Engineering, 13(4): 199-204. https://doi.org/10.1061/(ASCE)1084-0699(2008)13:4(199)

Toonen, W.H.J., Foulds, S.A., Macklin, M.G., Lewin, J., 2017. Events, episodes, and phases: Signal from noise in flood-sediment archives. Geology 45, 331–334. https://doi.org/10.1130/G38540.1

Toonen, W.H.J., Munoz, S.E., Cohen, K.M., Macklin, M.G., 2020. High-Resolution Sedimentary Paleoflood Records in Alluvial River Environments: A Review of Recent Methodological Advances and Application to Flood Hazard Assessment, in: Herget, J., Fontana, A. (Eds.), Palaeohydrology: Traces, Tracks and Trails of Extreme Events. Springer International Publishing, Cham, pp. 213–228. https://doi.org/10.1007/978-3-030-23315-0_11

U. S. Bureau of Reclamation, 2003. Flood Hazard Analysis: Seminoe and Glendo Dams Kendrick Project and Pick Sloan Missouri Basin Program, Wyoming, Tech. Serv. Cent., Denver.

U.S. Army Corps of Engineers, 1991. "Inflow Design Floods for Dams and Reservoirs," Engineer Regulation No. 1110-8-2 (FR).

Webb, R.H., O'Connor, J.E., Baker, V.R., 1988. Paleohydrologic reconstruction of flood frequency on the Escalante River. In: Baker, V.R., Kochel, R.C., Patton, P.C. (Eds.), Flood Geomorphology. John Wiley and Sons, N.Y., pp. 403–418.

Western Regional Climate Center, 2013. Cooperative Climatological Data Summaries. Retrieved from http://wrcc.dri.edu/climatedata/climsum/

Wilhelm, B., Ballesteros Cánovas, J.A., Macdonald, N., et al., 2019. Interpreting historical, botanical, and geological evidence to aid preparations for future floods. Wiley Interdiscip. Rev. Water 6, e1318. https://doi.org/10.1002/wat2.1318

Wintle, A.G. Murray, A.S., 2006. A review of quartz optically stimulated luminescence characteristics and their relevance in single-aliquot regenerative protocols: Radiation Measurements, v. 41, p. 369-391.

Wohl, E.E., Greenbaum, N., Schick, A.P., 1994. Controls on bedrock channel morphology along Nahal Paran, Israel. Earth Surf. Process. Landforms 19, 1–13.

World Meteorological Organization, 2009. Manual on estimation of Probable Maximum Precipitation (PMP), 3rd ed. World Meteorological Organization, Geneva.

Yevjevich, V., 1968. Misconceptions in hydrology and their consequences. Water Resour. Res. 4, 225–232. https://doi.org/10.1029/WR004i002p00225

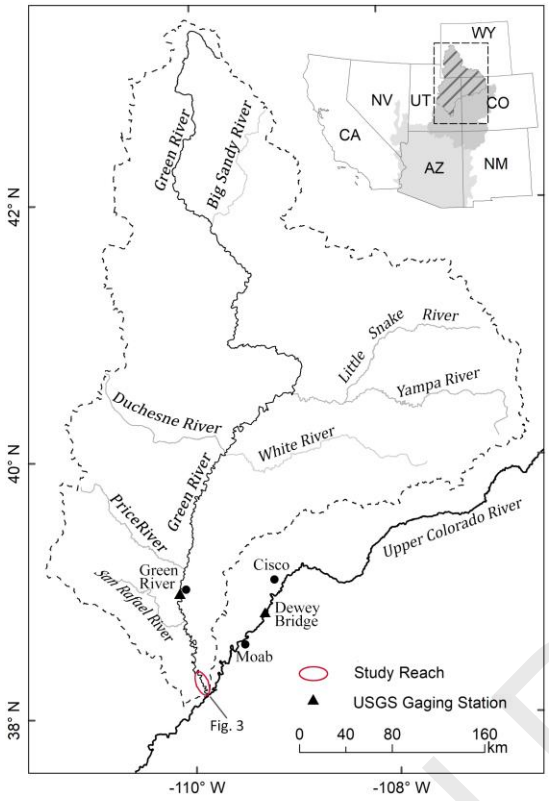

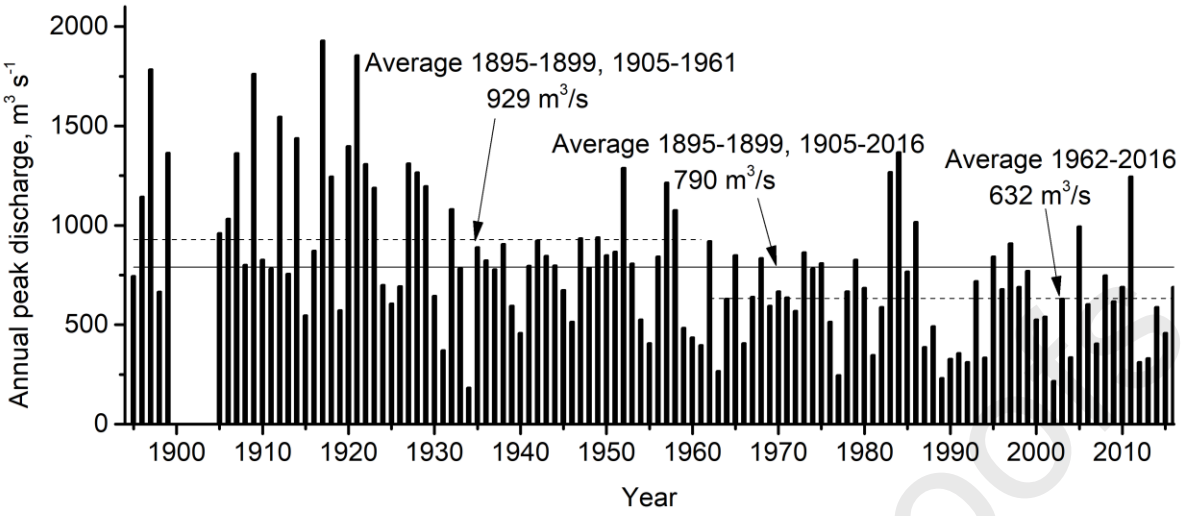

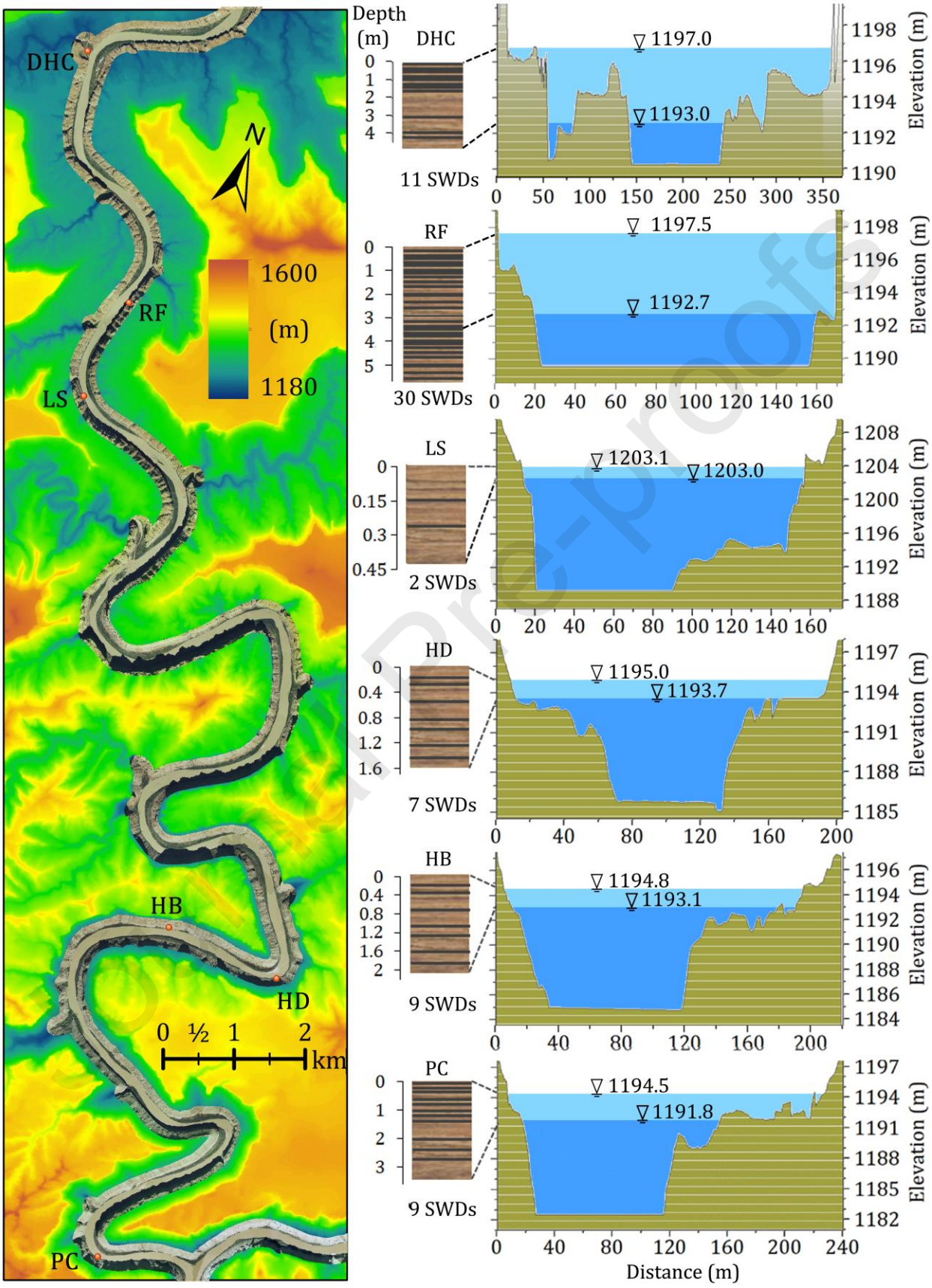

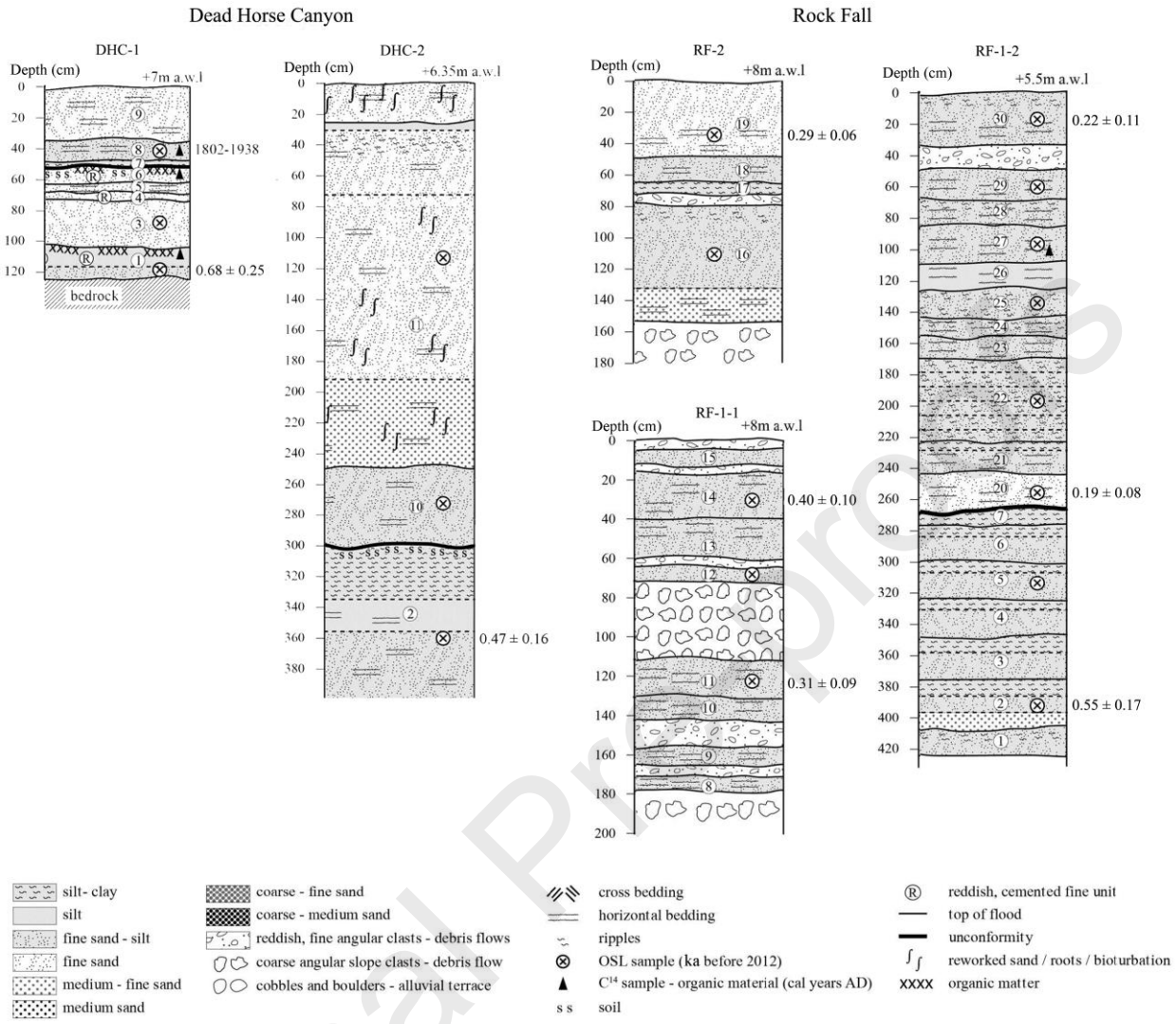

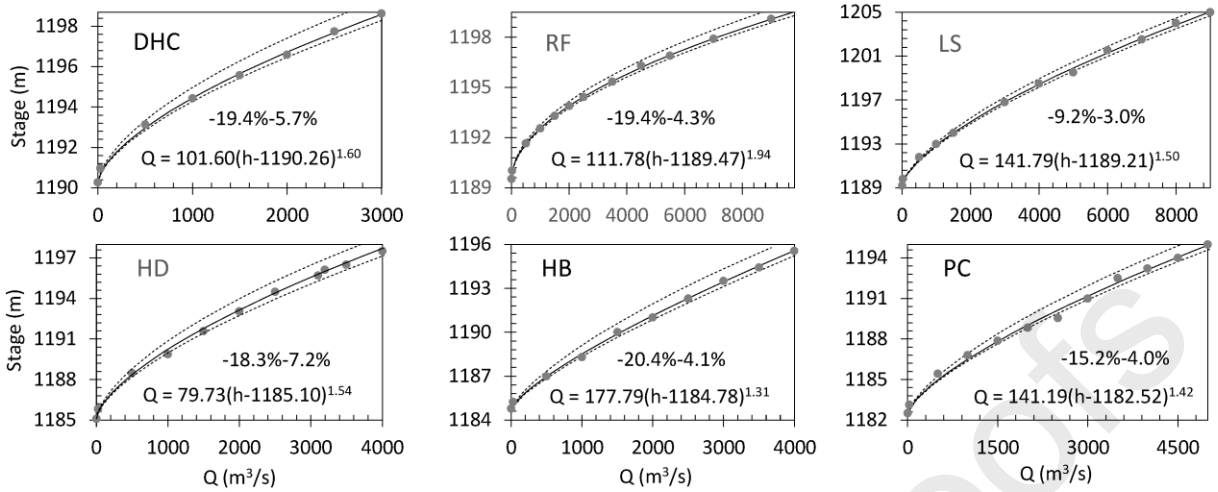

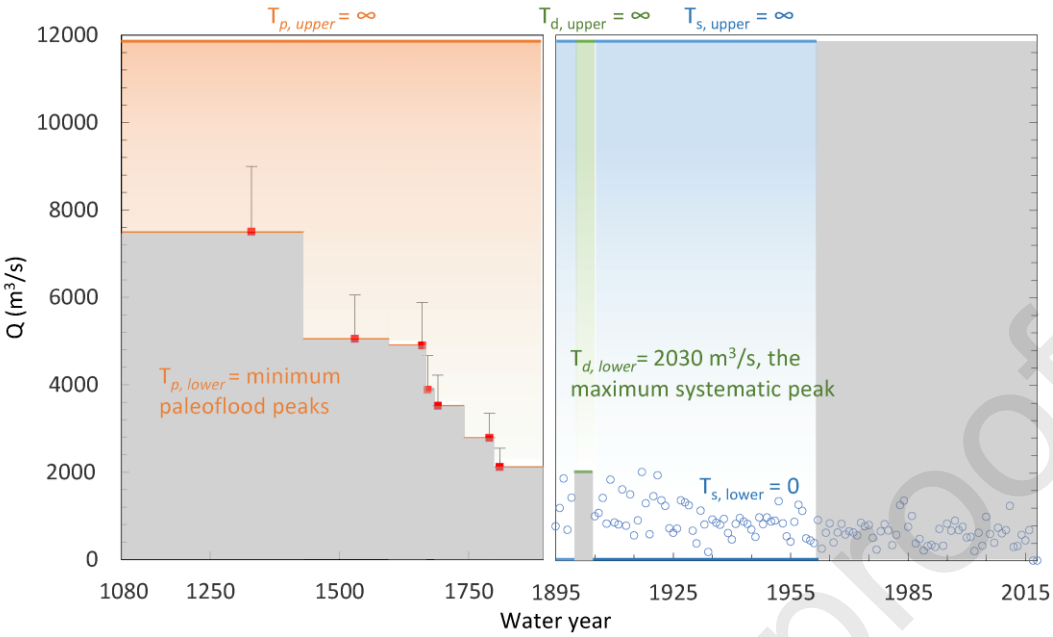

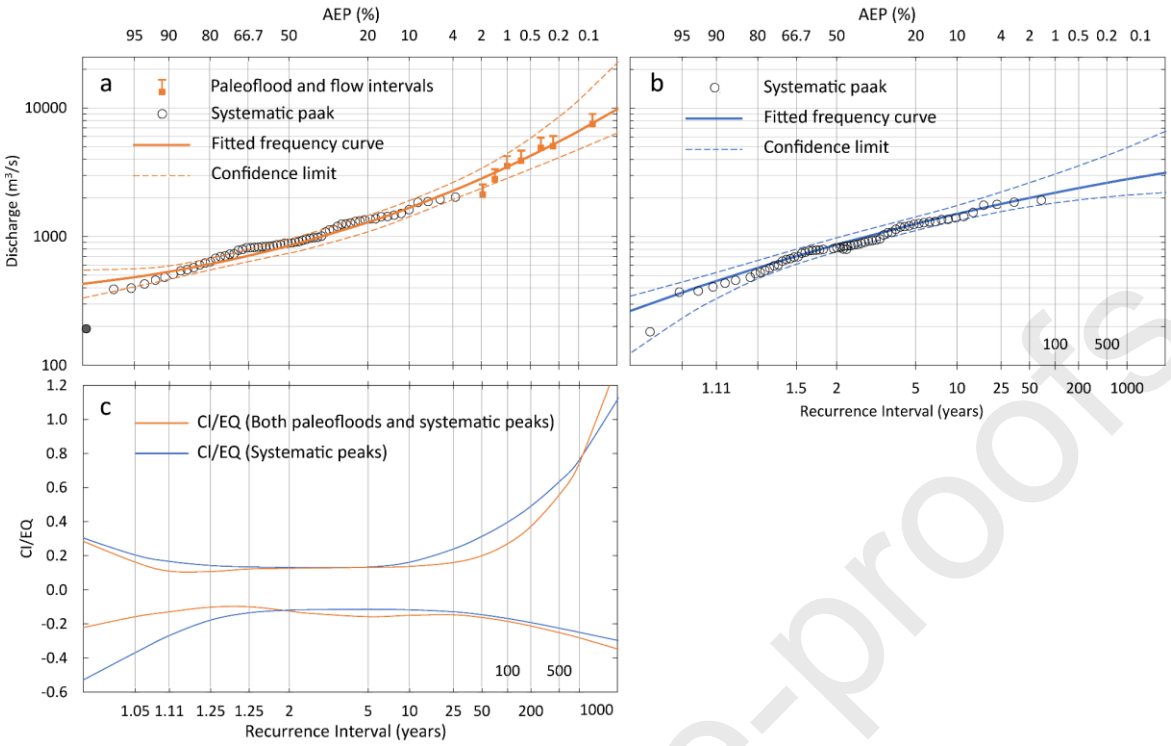

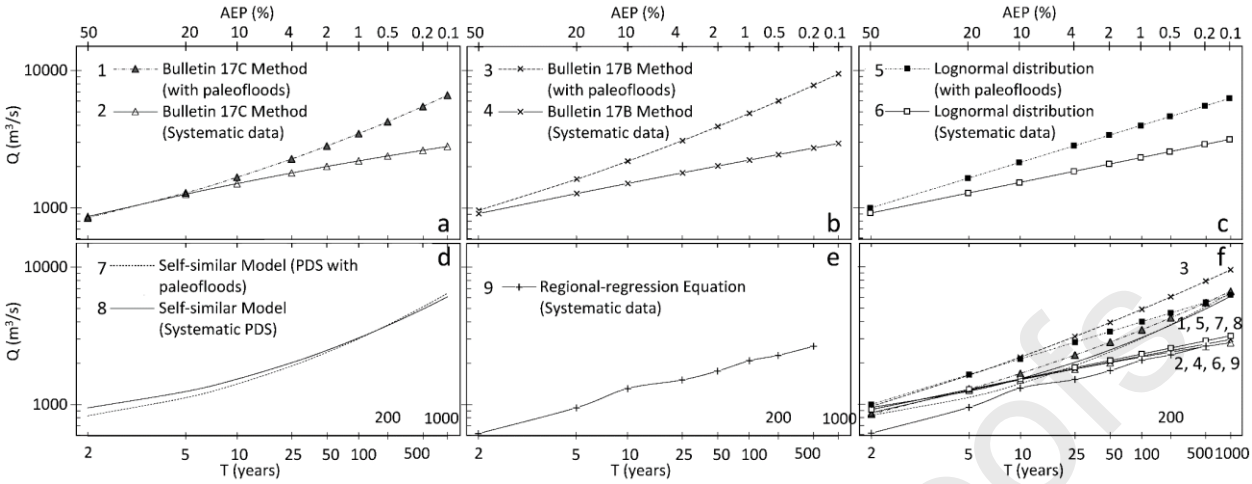

Figure 1. Green River Basin including the large tributaries, USGS gauging station, and the study reach.

Figure 2. Annual maximum peak discharges on the Green River at the USGS gauging station Green River, Utah, 1894-2016.

Figure 3. A map showing six study sites (DHC, RF, LS, HD, HB, and PC) on the Lower Green River (left), the stratigraphic illustrations showing the paleoflood slackwater deposit layers (black lines) and the river channel and valley dimensions of each stratigraphic section (middle), and the cross-sections at each site (right), showing the range of extreme flood water surface elevation.

Figure 4. Stratigraphic section at Dead Horse Canyon (DHC) site and Rock Fall (RF) site.

Figure 5. Particle tracings and water depths associated with sites of DHC, PC, HB, and HD on the Lower Green River. Areas of slack-water deposition develop through combinations of flow direction, speed, and depth. For sites location see figure 4.

Figure 6. Rating curves (solid lines) and corresponding results (dashed lines) for the 25% of Manning's n variation for six cross sections at the paleoflood sites on the Lower Green River. The sensitivity test shows an error of 3.0-20.4% can be introduced by the uncertainty of Manning's *n*.

Figure 7. Graph showing approximate systematic peak discharge and paleoflood estimates, with paleoflood exceedance thresholds, on the Lower Green River in the Stillwater Canyon reach. A scale break is used to separate the gaging station data from the much longer paleoflood record. Flood intervals for large floods in the paleoflood period are shown as red squares and black vertical bars with caps that represent minimum peaks and an additional 20% of the minimum. Mean values of paleofloods threshold age data are plotted for simplicity. Perception threshold ranges are shown as orange lines for the paleoflood period, blue lines for the systematic period, and green lines for the discontinued period. The gray shaded areas represents: (1) floods of unknown magnitude less than the perception thresholds for the paleoflood periods Tp,lower ; (2) the discontinued period Td,lower; (3) post-regulation floods after 1961.

Figure 8. Results of flood frequency analysis (FFA) using Expected Moments Algorithm (EMA) with Multiple Grubbs-Beck Test (MGBT) on the Lower Green River in the Stillwater Canyon reach, using (a) both systematic and paleoflood data; (b) systematic peaks solely. The solid line is the fitted log-Pearson Type III frequency curve and the dash lines are the 95% confidence limits. Peak discharge estimates from the gauge are shown as open circles; estimated paleoflood peak discharges are shown as solid squares; vertical bars represent estimated data uncertainty for paleofloods; the solid black circle is the potentially influential low flood (PILF) threshold as identified by the MGBT. Y-axis of the subplot (c), CI/EQ, is the ratio of confidence limits to expected quantiles.

Figure 9. Comparison of different techniques for flood frequency analysis (FFA) on the Lower Green River in the Stillwater Canyon reach, including systematic and paleoflood data. Subplots a-e include nine FFA curves using five techniques and all of them were synthesized in the subplot f. Annual exceedance probability (AEP), return period (T), and discharge (Q) for these curves are summarized in Table 7. The numbers refer to the discussion of each curve in the text and table. Note the partial duration series of the systematic data is used for self-similar model (subplot d).

Table 1. Characteristics of slackwater depositional environments for paleoflood SWDs in Stillwater Canyon of the lower Green River.

Stratigraphic section	Thickness (m)	SWD Layers	Texture	Top unit elevation (m a.w.l.)	Depositional environment
DHC-1	1.25	8	silt and fine sand	7.00	At a tributary mouth;
DHC-2	>4.00	4	clay, silt and fine sand	6.35	On a high rock ledge
RF-1-1	2.50	8	silt and fine sand	8.00	On the top of a rock-fall; Covered by stony colluvium
RF-1-2	4.20	18	clay, silt and fine sand	5.50	
RF-2	1.55	4	medium and fine sand	8.00	
LS	0.70	2	silt and fine sand	13.50	On a high rock ledge; Area of widening canyon
HD	1.50	7	silt and fine sand	10.00	Severe channel bend (>90°); Covered by stony colluvium
HB	2.00	9	clay, silt and fine sand	10.00	On the top of high alluvial terrace; Covered by stony colluvium
PC	>8.00	9	silt and fine sand	>12.00	Severe channel bend (>90°)

Table 2. Results of AMS 14C Dating of Paleoflood Deposits on lower Green River

Site, SWD Unit No.	Lab Sample no.	Type of dated material	Radiocarbon age (years BP)	Calibrated Age range (years AD)
DHC, #8	AA101614	Charred wood	90 ± 38	1681-1739 (26.6%) 1802-1938 (67.2%)
PC, #4	AA101615	Charred leaf	80 ± 39	1682-1736 (26.3%) 1805-1936 (69.1%)
PC, #5	AA101613	Charred bark	52 ± 38	1690-1730 (23.6%) 1810-1926 (71.8%)

Table 3. Results of OSL Dating of Paleoflood Deposits on lower Green River

Site, SWD Unit No.	Lab No.	Depth (m)	K (%)	U (ppm)	Th (ppm)	Cosmic (Gy/ka)	Dose rate (Gy/ka)	De (Gy)	Age ± 2σ (ka)
DHC-1, #1	GRV-2	1.00	1.66	1.9	6.0	0.19	2.58 ± 0.07	1.75 ± 0.64	0.68 ± 0.25
DHC-2, #2	GRV-3	4.00	1.74	2.5	8.0	0.13	2.68 ± 0.06	1. 25 ± 0.43	0.47 ± 0.16
DHC-2, #11	USU-2310	1.10	1.78	2.8	8.4	0.18	3.10 ± 0.14	0.61 ± 0.25	0.20 ± 0.08
RF-1, #2	GRV-11	4.00	1.66	3.0	10.7	0.13	2.63 ± 0.06	1.43 ± 0.44	0.55 ± 0.17
RF-1, #11	USU-2309	1.25	1.72	1.9	5.9	0.23	2.69 ± 0.12	0.85 ± 0.22	0.31 ± 0.09
RF-1, #14	GRV-9	0.30	1.66	2.8	7.8	0.23	3.00 ± 0.06	1.20 ± 0.30	0.40 ± 0.10
RF-2, #19	GRV-12	0.40	1.66	2.3	7.5	0.22	2.85 ± 0.07	0.83 ± 0.16	0.29 ± 0.06
RF-1, #20	USU-2307	2.60	1.74	2.6	9.0	0.19	3.08 ± 0.14	0.58 ± 0.24	0.19 ± 0.08
RF-1, #30	GRV-10	0.30	1.66	2.5	8.1	0.23	2.95 ± 0.06	0.64 ± 0.31	0.22 ± 0.11
LS, #2	GRV-6	0.30	1.58	1.4	4.6	0.23	2.36 ± 0.06	0.51 ± 0.10	0.22 ± 0.04
HB, #1	GRV-5	1.90	1.58	1.9	5.4	0.17	2.40 ± 0.06	1.07 ± 0.16	0.35 ± 0.07
HB, #8	GRV-4	0.30	1.66	2.2	7.0	0.23	2.80 ± 0.07	0.88 ± 0.07	0.32 ± 0.07
PC, #2	GRV-8	2.50	1.74	2.5	8.6	0.15	2.74 ± 0.08	0.94 ± 0.24	0.34 ± 0.09
PC, #7	USU-2306	0.55	1.56	2.0	6.7	0.24	2.65 ± 0.12	0.53 ± 0.26	0.20 ± 0.10
PC, #8	GRV-7	0.30	1.83	2.5	8.5	0.23	3.13 ± 0.08	1.51 ± 0.25	0.48 ± 0.17

Table 4. Results of the minimum paleoflood peak discharges using SHR-2D model with the percentage of variation resulting from a 25% change in the Manning's n values.

Site Name	Deposit unit	Water level during the LiDAR Flight (m)	Elevation above the water level (m)	Estimated peak stage (m)	Minimum peak discharge (m^3/s)	Variation
Dead Horse	DHC-9	1190.97	7.00	1197.97	2747	-14.3-6.2%
	DHC-8		6.65	1197.62	2558	-14.7-6.3%
	DHC-1		5.80	1196.77	2120	-15.5-6.5%
	DHC-2		3.00	1193.97	920	-17.7-6.9%
Rock fall	RF-19	1190.03	8.00	1198.03	7271	-13.1-4.8%
	RF-30		5.50	1195.53	3768	-16.1-5.5%
	RF-20		5.10	1195.13	3313	-16.5-5.5%
	RF-2		1.40	1191.43	507	-18.9-6.1%
Ledge Site	LS-top	1189.73	13.50	1203.23	7499	-6.4-4.9%
	LS-2		13.35	1203.08	7379	-6.5-4.9%
	LS-1		13.25	1202.98	7299	-6.5-4.9%
High Driftwood	HD-7	1185.82	10.00	1195.82	3207	-12.4-7.6%
	HD-1		8.40	1194.22	2520	-13.7-8.0%
High Bank	HB-9	1184.78	10.00	1194.78	3615	-11.6-4.4%
	HB-8		9.80	1194.58	3520	-11.8-4.5%
	HB-1		8.20	1192.98	2790	-13.6-5.1%
Powell Canyon	PC-9	1183.13	12.00	1195.13	5104	-9.3-4.1%
	PC-8		11.90	1195.03	5047	-9.4-4.1%
	PC-7		11.65	1194.78	4905	-9.6-4.2%
	PC-2		9.80	1192.93	3891	-10.7-4.3%

Table 5. EMA (Expected Moments Algorithm) flow intervals for the paleoflood and systematic records during 1080-2016 on the lower Green River, Utah.

Water Year	$Q_{Y,lower}$ (m^3/s)	$Q_{Y,upper}$ (m^3/s)	Comment
1330	7500	9000	
1530	5050	6060	
1660	4910	5890	For paleofloods, estimated peaks are minimal values; with an addition 20% as upper level for each estimation.
1670	3890	4670	
1690	3520	4220	
1790	2790	3350	
1810	2120	2540	
1895-1899	$Q_{Y,lower} = Q_{Y,lower} = Q_Y$		Gaged data are nearly exactly known equaling to measured value (Q_Y).
1905-1961			

Table 6. EMA (Expected Moments Algorithm) perception threshold for the paleoflood and historical period from 1080 to 1961 on the lower Green River, Utah.

Start Year	End Year	EMA perception threshold (m^3/s)		Comments
		$T_{Y,lower}$	$T_{Y,upper}$	
1080	1961	0	Infinity	Total Record
1080	1430	7500	Infinity	Top of paleoflood SWD
1431	1595	5050	Infinity	Top of paleoflood SWD
1596	1665	4910	Infinity	Top of paleoflood SWD
1666	1680	3890	Infinity	Top of paleoflood SWD
1681	1740	3520	Infinity	Top of paleoflood SWD
1741	1800	2790	Infinity	Top of paleoflood SWD
1801	1894	2120	Infinity	Top of paleoflood SWD
1895	1899	0	Infinity	Systematic data
1900	1904	2030	Infinity	Broken; Largest systematic data
1905	1961	0	Infinity	Systematic data

Table 7. A comparison between flood frequency results using different methods on the lower Green River, Utah (in m^3/s). The regional-regression based 1000-yr flood is not provided in Kenney et al. (2007).

No.	Method	Return Period (yrs)								
		2	5	10	25	50	100	200	500	1000
1	Bulletin 17C Method (with paleofloods)	847	1289	1671	2274	2825	3475	4245	5483	6616
2	Bulletin 17C Method (Systematic data)	867	1259	1504	1798	2004	2201	2389	2628	2801
3	Bulletin 17B Method (with paleofloods)	962	1623	2196	3101	3925	4894	6032	7845	9487
4	Bulletin 17B Method (Systematic data)	913	1275	1511	1806	2023	2238	2452	2736	2954
5	Lognormal distribution (with paleofloods)	995	1641	2132	2818	3374	3968	4602	5507	6247
6	Lognormal distribution (Systematic data)	914	1279	1526	1840	2078	2317	2560	2888	3144
7	Self-similar Model (PSD with paleofloods)	828	1121	1409	1907	2398	3015	3791	5131	6451
8	self-similar Model (Systematic PSD)	945	1243	1531	2014	2479	3052	3756	4944	6085
9	Regional-regression Equation (Systematic data)	615	949	1308	1509	1753	2082	2283	2654	

High Lights:

- A comprehensive paleoflood investigation on the lower Green River, Utah.
- At least 27 extreme floods in the past 700 years were retrieved.
- Extreme floods are larger and more frequent than implied by gauged records.
- A truly scientific understanding of extreme floods can only emerge from nature.